Measuring drift velocity and electric field in mirror machine by fast photography

2013 JINST 8 P02005

(http://iopscience.iop.org/1748-0221/8/02/P02005)

PUBLISHED BY IOP PUBLISHING FOR SISSA MEDIALAB

RECEIVED: *December 13, 2012*
ACCEPTED: *January 11, 2013*
PUBLISHED: *February 12, 2013*

2013 JINST 8 P02005

Measuring drift velocity and electric field in mirror machine by fast photography

I. Be'ery,[a,1] **O. Seemann,**[a] **A. Fruchtman,**[b] **A. Fisher**[a] **and J. Nemirovsky**[a]

[a] *Physics Department, Technion – Israel Institute of Technology, Haifa 32000, Israel*
[b] *Faculty of Sciences, H.I.T. – Holon Institute of Technology, Holon 58102, Israel*

E-mail: ilanbeery@gmail.com

ABSTRACT: The flute instability in mirror machines is driven by spatial charge accumulation and the resulting E×B plasma drift. On the other hand, E×B drift due to external electrodes or coils can be used as a stabilizing feedback mechanism. Fast photography is used to visualize Hydrogen plasma in a small mirror machine and infer the plasma drift and the internal electric field distribution. Using incompressible flow and monotonic decay assumptions we obtain components of the velocity field from the temporal evolution of the plasma cross section. The electric field perpendicular to the density gradient is then deduced from E=-V×B. With this technique we analyzed the electric field of flute perturbations and the field induced by electrodes immersed in the plasma.

KEYWORDS: Image processing; Plasma diagnostics - high speed photography

[1] Corresponding author.

doi:10.1088/1748-0221/8/02/P02005

Contents

1 Introduction

The flute (interchange) instability is governed by an internal positive feedback: deviation from symmetric plasma shape leads to charge accumulation, and the resulting electric field drives the asymmetry further. The first study of active feedback control of plasma instability [1] considered the use of many electrodes at the plasma's outer diameter to reverse the positive feedback. Early works applied active feedback to mirror traps with a major improvement of plasma density [2, 3]. These experiments used electrodes to sense the plasma's electric field and other electrodes as actuators to feed back an external field. The plasma density in these experiments was low enough so that the plasma relative dielectric constant was close to 1, and the electric fields were similar to the vacuum fields.

Another stabilization mechanism based on external electric field is the 'vortex confinement' [4]. In this method a voltage is applied between several annular electrodes in contact with the plasma at different radii. The imposed radial electric field drives rotation at the outer layer of the plasma, which stabilized all the flute modes higher than $m = 1$. Vortex confinement is used at the GDT (Gas Dynamic Trap) facility [5] with plasma of a medium temperature and high β (the ratio of plasma to magnetic pressures). The potential distribution and the resulting electric field due to the annular electrode were measured in this experiment using floating probes [5].

Fast photography has been used to study interchange and drift instabilities in both toroidal and linear plasma experiments [6–8]. In these works the images are usually analyzed by techniques of image recognition, spectral analysis, or just qualitative observations.

The present work employs fast video photography to track the evolution of the plasma shape. Using few assumptions, the plasma drift velocity parallel to the density gradient and perpendicular

2013 JINST 8 P02005

to the axis of symmetry can be deduced from the measured plasma motion. This velocity can then be translated to the electric field perpendicular to the density gradient and perpendicular to the axis of symmetry. This technique is used for studying the electric field in two cases: free evolution of flute instability and small biased electrodes intended as feedback actuators.

Section 2 describes the experimental apparatus and the main plasma parameters. In section 3 we discuss the conditions which allow us to assume that the plasma flow between consecutive frames is incompressible. We further show that the measured luminosity "flow" can be also described by incompressible flow continuity equation. In section 4 we describe how to extract the parallel velocity field and the perpendicular electric field from the measured plasma evolution. In section 5 we bring two examples of the obtained fields in the cases of free flute evolution, and external electrodes. Section 6 summarizes the results and discusses the applicability to other experiments.

2 Experimental apparatus

The experiments were performed in a table-top mirror machine with a vacuum chamber inner diameter of 12.5 cm and 40 cm distance between the magnetic mirrors (figure 1). The magnetic field at the middle of the trap ranges from 0.05 T to 0.2 T, and the maximal mirror ratio is 20. Plasma is injected into the trap from a capillary plasma gun [9] located outside one of the mirrors. The capillary gun is based on high voltage surface discharge in a polypropylene capillary. The gun injects almost pure hydrogen plasma into the trap with a temperature of 3–5 eV, an axial velocity of 2–3 cm/μs, and density higher than 10^{13} cm^{-3} at the center of the trap. The gun discharge current diminishes after less than 3 μs, and the plasma reaches the opposite end of the trap within about 15 μs. The plasma persists for another 40 μs before it decays beyond the camera's sensitivity. At this interval the plasma can be treated as sourceless for the following analysis.

Six hemispherical electrodes are located at the periphery of the plasma (figure 1). Each electrode can be individually biased with a voltage up to 600 V to induce an electric field and plasma flow with a pre-determined geometry.

Most of the photography in the present study was taken with a Phantom V710 camera. This CCD camera can take 100×100 pixels images with 3.8 μs between frames or larger images at a slower frame rate. At the higher frame rate there are 7–10 workable frames for each discharge between plasma injection and decay to the noise level. The images were taken along the axis of the trap through a glass window opposing the plasma gun. We used the red channel of the camera as a broad filter to separate the H_α radiation for image processing. Spectroscopic measurements indicate that except for a small region at the throat of the plasma gun, the radiation from the plasma is almost purely H_α and H_β.

While we intend to measure the plasma density, $\rho(r,\theta)$, in a plane perpendicular to the magnetic field, we actually measure a projection along the z-direction of the recombined neutral Hydrogen. We claim that our measurement is a good approximation to the plasma density distribution in the center of the trap, based on two arguments: first, the projection of the density is almost identical (up to a multiplying factor) to the density distribution at the center of the trap. This is due to the elongated geometry of the plasma column which makes the contribution of the mirrors region to the total collected light small and affects only the center of the image. Second, we can treat

2013 JINST 8 P02005

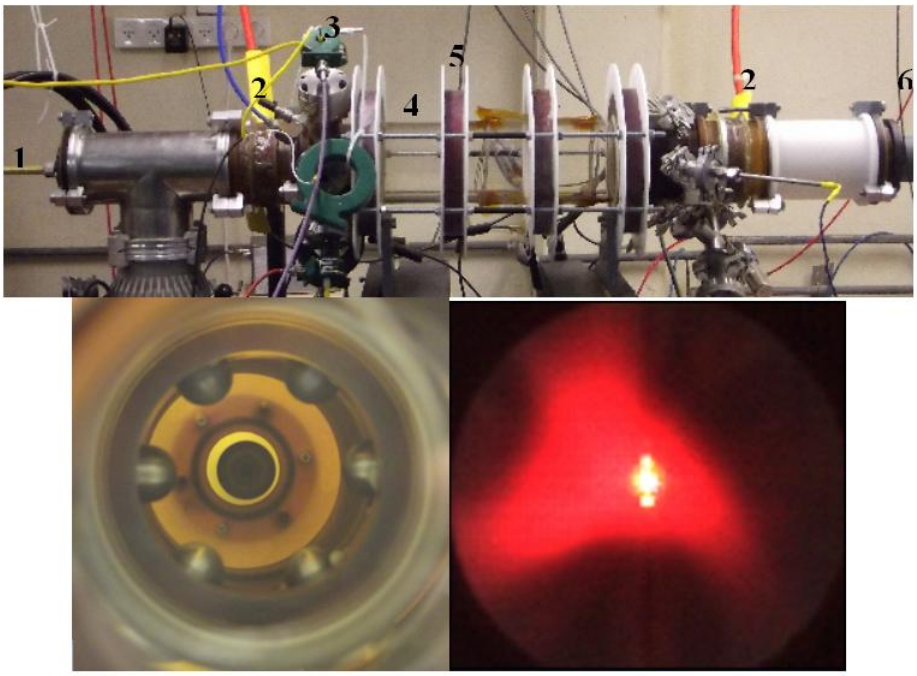

Figure 1. Top — overview of the experiment showing plasma gun (1), mirror coils (2), electrodes ports (3), glass chamber (4), shaping coils (5), viewing window (6). Bottom — static image showing the field of view of the camera with gun tip at the center surrounded by six electrodes (left), and a typical dynamic image (right).

the H_α as a marker to the local plasma density. The typical distance a Hydrogen atom propagates between recombination to the emission of H_α photon is$\Delta = V_{th}\tau_{\text{decay}}$, where $V_{th} \approx 2\,\text{cm}/\mu s$ is the typical thermal velocity and $\tau_{\text{decay}} \approx 0.1\mu s$ is the radiative decay time, as determined from Einstein coefficients [10]. Thus, we see that Δ is much smaller than the plasma radius.

Another problem with measuring the H_α radiation is that it is not necessarily proportional to the plasma density, ρ. The relation between H_α intensity and plasma density depends on the mechanism that generated exited Hydrogen atoms: it can be n^2 for collisional excitation or 2-body recombination, or it can be n^3 for 3-body recombination. We show in section 3.2 that we do not need to know the exact relation between H_α intensity and plasma density as long as we know that this dependence is monotonic and the intensity depends only on the density. This is true in our system, but it might not apply to other systems. For example in experiments that use neutral puffing to view the plasma [6] the luminosity depends both on the plasma density and the density of the puffed neutrals. Generally, the plasma luminosity depends on temperature as well as density. In the following analysis it is assumed that the plasma temperature is homogeneous because the plasma is originated in a very dense, non-magnetized capillary discharge, and because the duration of the experiments is short compared to any cooling process other than collisions with the walls. Note that temperature gradients can be tolerated in the following analysis, as long as it does not alter the monotonic dependence of luminosity on density and the characteristic cooling time is large relative to the time between consecutive frames (3.8 μs).

2013 JINST 8 P02005

3 Incompressible flow of luminosity

In section 4 it is assumed that the measured luminosity is "flowing" according to incompressible continuity equation. The present section first discusses the necessary conditions for the assumption of incompressible flow of plasma. It then shows that under few general assumptions, the incompressible flow of plasma implies the observed incompressible flow of luminosity.

3.1 Incompressible flow of the mass density

The continuity equation for the mass density, ρ, is:

$$\frac{\partial \rho}{\partial t} + \nabla \cdot \left(\vec{V} \rho \right) = \frac{\partial \rho}{\partial t} + \vec{V} \cdot \nabla \rho + \rho \nabla \cdot \vec{V} = S, \tag{3.1}$$

where $\vec{V}$ is the plasma velocity, and S, is the source term. It is a common assumption that the plasma is incompressible during the evolution of the flute instability. This is because, as stated in [11], the potential energy of the plasma in the curved magnetic field is usually insufficient to provide the increase in the thermal energy or the increase in the magnetic field energy when either the plasma or the magnetic field is compressed. The condition for incompressibility is derived in [11] for small two-dimensional perturbations in a slab geometry. The equivalent condition for small two-dimensional perturbations in a cylindrical geometry is$1/k\tau \ll v_A$, where τ is a characteristic timescale of the perturbation, $k = m/2\pi r_p$ is the azimuthal wave number with m and r_p the mode number and plasma radius, and v_A is the Alfven velocity. The inequality is indeed satisfied in our system for m$\geqslant$1. If the plasma evolves as a result of the flute instability, the characteristic time should be $\tau = 1/\gamma$ where the growth rate γ is [11] $\gamma \approx \sqrt{-2p'/\rho R_c}$. Here R_c is the radius of curvature of the magnetic field, p is the plasma pressure, and p' is a characteristic pressure radial gradient. For such a timescale, the above condition for incompressibility becomes$\beta \ll k^2 r_p R_c$. In our system $\beta \approx 0.01$, $m = 1 \ldots 5$, $r_p \approx 4$ cm, and the field line averaged R_c is more than 100 cm, so the last condition easily holds.

A possible source for compressible plasma flow is diffusion across the magnetic field. The typical diffusion time constant is$\tau_{\text{diff}} = 1/Dk^2$, where D is the diffusion coefficient. In linear mirror machines the relevant diffusion processes are Bohm diffusion and classical diffusion. The diffusion time for Bohm diffusion is typically larger than 200 μs in our experiment, while the classical diffusion time is even larger. Both diffusion times are much larger than the typical flute growth time of 10–20 μs. Therefore, the effect of the diffusion on the incompressible assumption is relatively small.

Following the considerations detailed above, we neglect the compressibility term in equation (3.1), $\rho \nabla \cdot \vec{V}$, to obtain:

$$\frac{\partial \rho}{\partial t} + \vec{V} \cdot \nabla \rho = S \tag{3.2}$$

While the incompressible flow assumption is a good global approximation, there are regions in the observed flow that are not described adequately by equation (3.2). These are the regions where the density gradient is very small, or the velocity is perpendicular to the density gradient, so the convection term, $\vec{V} \cdot \nabla \rho$ is very small and might become comparable to the compressibility term. Note that these two conditions mean that the plasma flow produces only small changes in the

2013 JINST 8 P02005

observed density. Therefore, in areas where the measured density change is relatively small, the credibility of the obtained velocity is low, while the credibility is higher where the relative density change is high.

3.2 The continuity equation for the luminosity

We argued that the density flow is approximately incompressible. We now show that if the luminosity is monotonically dependent on the density, then the luminosity obeys the same continuity equation with a different source term.

Let us assume the plasma luminosity is $L = \xi(\rho)$, where ξ does not depend explicitly on time or space, and is monotonic in ρ. The arguments for this assumption are discussed in section 2. This means there is an inverse monotonic function,$\rho = \xi^{-1}(L)$. Putting it into the incompressible flow results in:

$$\frac{\partial \xi^{-1}(L)}{\partial t} + \vec{V} \cdot \nabla \xi^{-1}(L) = S \tag{3.3}$$

Using the chain rule, $\frac{\partial \xi^{-1}(L)}{\partial t} = \frac{\partial \xi^{-1}}{\partial L}\frac{\partial L}{\partial t}$, and $\nabla \xi^{-1}(L) = \frac{\partial \xi^{-1}}{\partial L}\nabla L$. This results in the continuity equation for the luminosity:

$$\frac{\partial L}{\partial t} + \vec{V} \cdot \nabla L = S / \frac{\partial \xi^{-1}}{\partial L} = S\frac{\partial L}{\partial \rho} = S' \tag{3.4}$$

There are three observations about S' that are needed for the next section. First, since $\frac{\partial L}{\partial \rho}$ is independent of the location, the locality of S dictates the locality of S'. Second, if $S = 0$ then $S' = 0$ and vice versa. Third, since both the luminosity and the decay rate depend in a similar manner on the recombination rate, we assume that in our experiment, S and S' are always negative and depend only on the mass density and luminosity respectively.

4 Elimination of the source term and calculation of $\mathbf{V}_{||}$ and $\mathbf{E}_{\perp}$

In order to deduce the plasma motion and electric field from the comparison of consecutive images, we need to employ the following assumptions, which have been discussed in the previous sections:

1. The measured plasma projection is proportional to the plasma density distribution at the trap's center.
2. The local luminosity in the images is monotonically dependent on the plasma density, ρ.
3. The plasma β is small. This implies that the magnetic field in the plasma is the magnetic field of the trap: $\vec{B} \cong B_{0z}$. Measurements with diamagnetic loops indicate that β in our experiments is usually in the range 0.01–0.1.
4. The plasma flow is incompressible.

In the previous section we established that the observed luminosity obeys a continuity equation (3.4). Looking at two consecutive frames (figure 2), it is clear that the plasma decays, resulting in a large source term. Generally S' includes any sink / source term: injection, recombination, diffusion, etc. In our system, after the initial plasma injection, the dominant process contributing

2013 JINST 8 P02005

to S' is recombination. This process has a special advantage for the present analysis: it depends only on the local plasma density and it only decreases the plasma density. This means that while the density and luminosity in each plasma element changes between consecutive frames, there is a unique function that translates the density and luminosity in one frame to the next one. By finding this function and correcting the intensities in the second frame to those of the first frame we practically annihilated the source term, S'. In simpler terms, we argue that the brightest plasma element in the first frame stays the brightest element in the next frame although its location and intensity might change, and the same is true for the second brightest plasma element and so forth. Therefore, if we order the pixels in each frame by their intensity (i.e. cumulative histogram) we can see how the intensity of each plasma element changed between the frames and correct the intensity in the second frame to that of the first.

Figure 2 demonstrates this procedure. The top of the figure shows the accumulated mass density (integration of the histogram) of two consecutive frames. We refer to these function as $L_i(N)$, where N is the number of pixels with luminosity greater than L, and i is the index of the frame. Clearly, for every N, the function $L_2(N)$ (of the second frame) is lower than the function $L_1(N)$ (of the first frame) due to plasma decay. However, the histogram of the second frame can be recalibrated by multiplying the density of each pixel in the second frame by: $\frac{L_1(N)}{L_2(N)}$. Based on the uniqueness of the relation between L_1 and L_2, recalibrating the accumulated mass in such a way is equivalent to setting S=0 in the continuity equation. The bottom of figure 2 demonstrates the effect of recalibration of the second frame in such a manner. Before the recalibration the luminosity (expressed as color) of the plasma at the second frame is markedly lower, while after the recalibration the intensities are the same and only the drift is observed.

If more than two frames are analyzed in a single discharge one can recalibrate the later frames based on the anchor of the first frame, $\frac{L_1(N)}{L_n(N)}$, or individually for each two consecutive frames, $\frac{L_{n-1}(N)}{L_n(N)}$. It is found that the latter option usually generate more reliable results, probably because it avoids accumulation of errors.

After setting S=0, we can write the continuity equation as:

$$\frac{\partial L}{\partial t} \cong \frac{\Delta L}{\Delta t} \cong -\vec{V} \cdot \langle \nabla L \rangle \tag{4.1}$$

where ΔL is the local change in luminosity between the frames, Δt is the time between frames, and $\langle \nabla L \rangle$ is the luminosity gradient, averaged over the two frames. Re-arranging we obtain:

$$\vec{V}_{||} = \frac{\Delta L}{\Delta t \, \| \langle \nabla L \rangle \|} \cdot \vec{u}_{\nabla L} \tag{4.2}$$

Here $\vec{u}_{\nabla L}$is a unit vector in the direction of the local gradient in luminosity, and $\vec{V}_{||}$ is the velocity parallel to the luminosity gradient and perpendicular to the magnetic field. Since all these values can be calculated from the image, it is now possible to find$\vec{V}_{||}$.

The parallel velocity is used to derive the electric field perpendicular to the luminosity gradient and perpendicular to the magnetic field. Under the assumption that the bulk plasma motion is governed solely by ExB drift, the electric field can be calculated from the velocity by: $\vec{E} = -\vec{V} \times \vec{B}$. Taking again $\vec{B} = B_{0z}$ and $\vec{V} \cdot \vec{B} = 0$, which simplifies the expression of the electric field to:

$$\vec{E}_{\perp} = -\vec{V}_{||} \times \vec{B} = -\vec{V}_{||} B_{0z} \tag{4.3}$$

2013 JINST 8 P02005

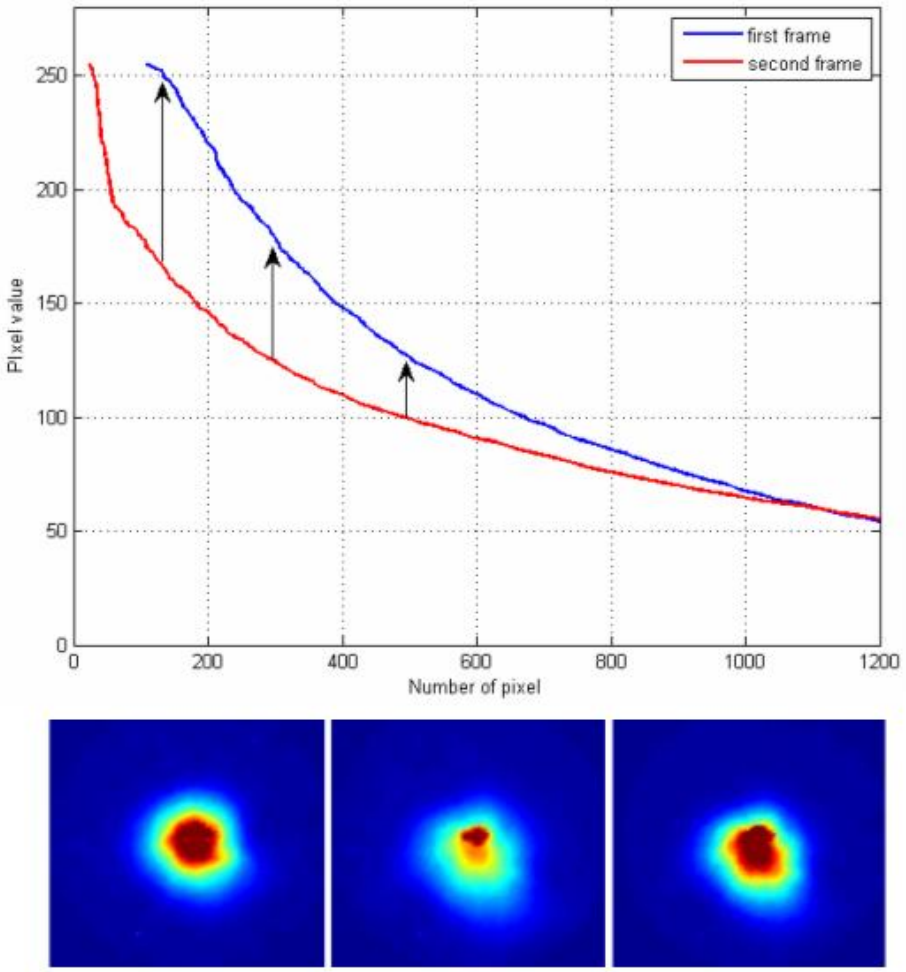

Figure 2. Top: accumulated mass density of two consecutive frames. The arrow indicate the effect of recalibration. Bottom from left to right: the first frame, second frame, and the second frame after recalibration. The color pallet is the same for all the frames.

Figure 3 illustrate how eqs. (4.2) and (4.3) are used to extract the plasma velocity and the electric field. At a small region at the center of both images the CCD is saturated, so the difference and gradient of luminosity cannot be estimated there. The plot of ΔL (top left of figure 3) shows that in this particular case the plasma is mostly drifting down, resulting in plasma luminosity increase at the bottom and decrease at the top. The gradient of the luminosity (top right of figure 3) is the average of the gradient in the two frames. The parallel velocity and perpendicular electric fields are demonstrated by a quiver plot (bottom of figure 3), where the direction of the arrows is the direction of the local field, and the size of the arrows indicate the magnitude of the field. Note in this example the velocity seems to decrease to a very low value near the vertical center of the plasma (around pixel 50 in the vertical scale). This is because the luminosity gradients in this region is mostly horizontal while the velocity of the plasma is mostly vertical so $\left|\vec{V}_{||}\right| \ll \left|\vec{V}\right|$. The derived electric field points mostly in the horizontal direction. This field is a result of $m = 1$ electrode biasing, as described later in section 5.2.

2013 JINST 8 P02005

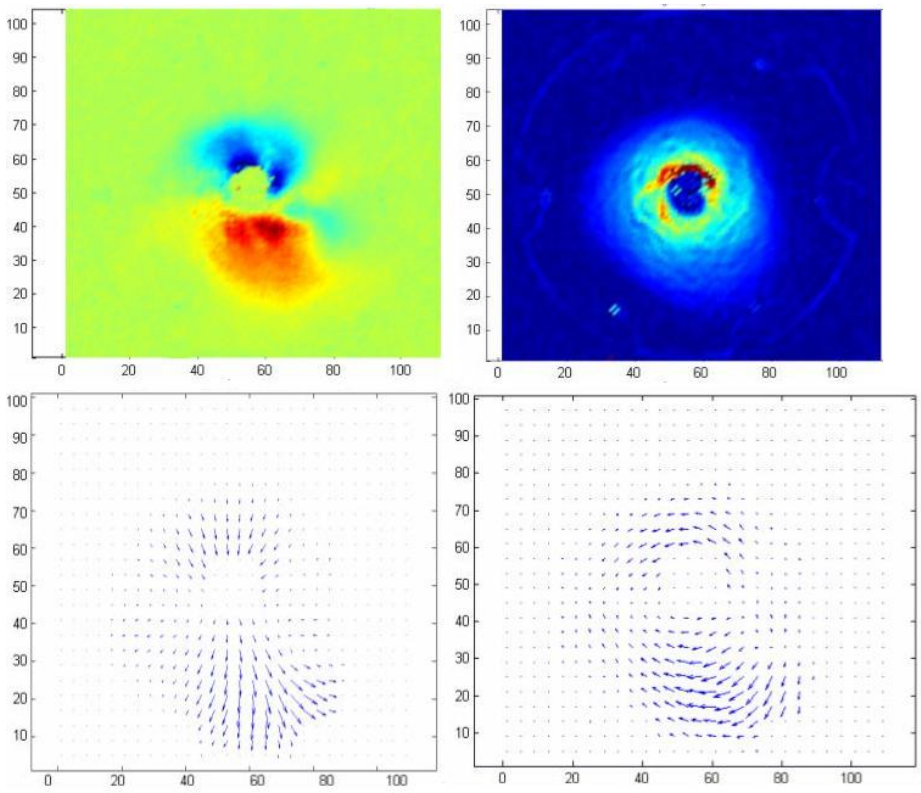

Figure 3. Top-left: difference between consecutive frames. Red corresponds to the second frame being brighter, while blue corresponds to the first frame being brighter. Top-right: magnitude of gradient. Bottom-left: quiver plot of the derived velocity field, $\bar{V}_{||}$. Bottom-right: derived electric field, $\bar{E}_{\perp}$.

5 Experimental results

5.1 The electric field of flute instability

In low β plasma, the flute instability can be described as a positive feedback where an azimuthal asymmetry of the plasma cross-section induces charge accumulation due to centrifugal drift, and the accumulated charge increases the asymmetry by E×B drift. Our method suggested here enables us to measure both the plasma density distribution and the electric field from a photographed frame sequence. Figure 4 shows the electric field associated with the growth of perturbations in a typical experiment. For comparison figure 4 also includes the electric field in an MHD simulation of flute perturbation. The simulation is based on integration of 2-fluids drift equations in 2-dimensional, constant magnetic field with circular limiter. The simulation includes effective curvature drift current that drives the instability, and finite-Larmor-radius effect that partly stabilizes it. In these figures the sign (and color) of the electric field is determined relative to the direction of the density gradient. Positive (red) values correspond to field that cause plasma outflow, while negative (blue) corresponds to field that cause plasma inflow.

Since the flute is random in nature, it is difficult to make exact comparison with simulation, but two general conclusions can be drawn from observations of several experiments and simulation with various initial conditions:

2013 JINST 8 P02005

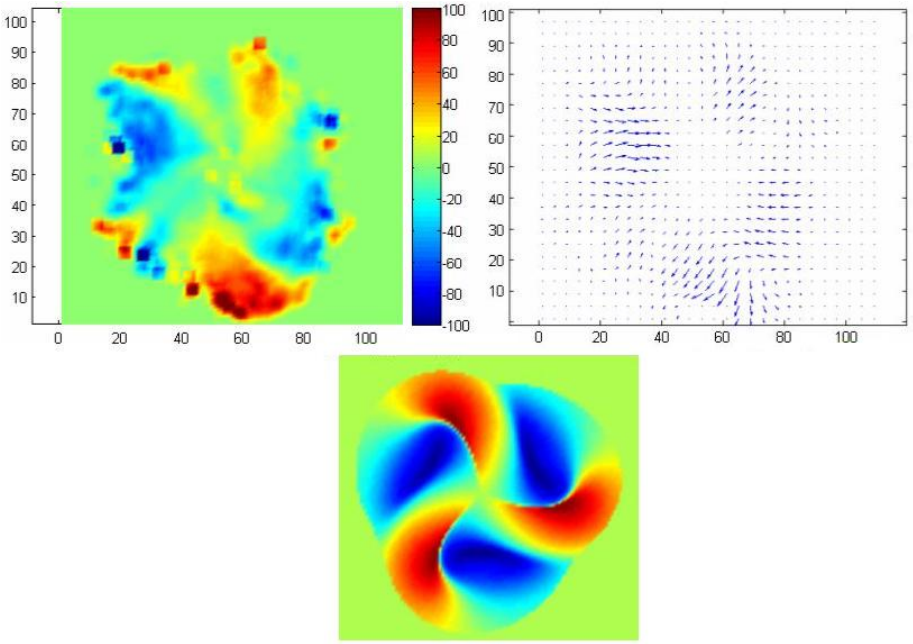

Figure 4. Top: magnitude of the electric field (left) and the quiver plot (left) of a developed flute instability, just before it reaches the vessel's wall. Bottom: simulated perpendicular electric field of flute perturbation with $m = 3$.

1. The electric field is maximal near the periphery of the plasma, where both the radial and azimuthal gradients are high. This is because the magnetic curvature and the density gradients are maximal at these regions. The gradient of the dielectric constant, which is not included in the simulation, further concentrates the electric field at the periphery of the plasma.

2. The electric field of the instability in the experiments reaches 100 V/m when the plasma reaches the wall. Taking B_{0z}=0.1 T, this field corresponds to drift velocity of about 1 mm/μs. Such velocities are indeed observed at the "fingers" of the perturbations.

The amplitude of the electric field, the relatively slow rotation, the limited number of unstable modes and the growth rate, all suggest that the perturbations are due to centrifugally-driven flute instability [12].

The electric field of the flute instability evolves in the linear regime as$E = E_0 e^{\gamma t}$, and the radial amplitude of the perturbation evolves as $\tilde{r} = \tilde{r}_0 e^{\gamma t}$. From the evolution of the plasma shape one can extract $e^{\gamma t}$ and then find the initial electric field at the time of plasma formation. For example, the image in figure 4 corresponds to $e^{\gamma t} \approx 20$, and therefore $E_0 \approx 5V/m$. This initial field can be attributed to fluctuations in the plasma formation process at the plasma gun.

5.2 Electric field due to electrodes

In order to measure the electric field induced in the plasma, the external electrodes were biased with constant voltage. The voltage had symmetry that corresponds to modes $m = 1, 2$ or 3 (figure 5.2). At low electrode voltage the plasma evolution remains mostly random, while at higher voltage the electrodes force the evolution of the flute mode that is consistent with their bias symmetry. The

2013 JINST 8 P02005

minimal voltage necessary for consistent m-seeding ranges from 100 V for $m = 1$ to 300 V for $m = 3$.

Figure 5.2 demonstrate typical velocity field and induced electric field in the case of 400 V $m = 3$ electrodes bias. For comparison we also bring in figure 5.2 the calculated azimuthal electric field for the same geometry and bias, but without the plasma. Comparing these fields one can see that they have similar symmetry, but the field in the plasma is smaller by two orders of magnitude relative to the vacuum field. The suppression of the electric field in the plasma can be attributed to gradients in the dielectric constant. The low frequency dielectric constant of magnetized plasma is [13]:

$$\varepsilon = 1 + \frac{\rho}{B} \tag{5.1}$$

For B=0.1 T and 10^{13} cm^{-3} Hydrogen ions, the above equation gives$\varepsilon \approx 10^6$. If the plasma density is lower by a factor of $\sim$100 near the electrodes relative to the areas which are visible to the camera, the same factor can be expected between the vacuum field and the field in the plasma. Note that the low electric field at the dense plasma implies a much stronger field near the electrodes, and that the electric field increases the ions Larmor radius by $R_L = E/B\Omega_{Ic}$, where Ω_{Ic} is the ion cyclotron frequency. As a result, the last few millimeters of the plasma near the electrodes are poorly magnetized. This explains the relatively high current measure between the electrodes, which can reach up to 30 A for bias of 400 V.

Figure 5.2 demonstrates that the field in the plasma is rotated relative to the electrodes. This is due to the rotation of the plasma in the ion diamagnetic current direction (corresponding to the plasma being positively-charged relative to the surrounding). Some shearing can also be observed in figures 5 and 6 due to differential angular velocity. Another observation, which is typical to most of the experiments, is that the field that drives the plasma outward (red colors) is stronger than the field driving the plasma inward (blue colors). This is the result of a positive feedback mechanism in which the outward field pulls the plasma into the spacing between the electrodes, where the field is maximal.

6 Conclusions

In this work we have demonstrated a method to calculate components of the velocity field and corresponding components of the electric field of the flute instability in a mirror machine. The analysis employs the continuity equation with several assumptions and manipulations that eliminated the compressibility and source terms. While in the current work applies the analysis method for optical images in linear mirror machine, the same analysis method can be applied to other plasma geometries, and other diagnostic tools that measure the evolution of the plasma distribution. For example, it can be used on tomographic reconstructions of the density distribution in tokomak using X-ray detectors [14].

The electric field obtained for flute perturbation using the described method is consistent with the amplitude and general features expected for this type of instability in our system. The electric field introduced by external electrodes is attenuated by two orders of magnitude relative to the vacuum field. The reduction is probably due to the dielectric constant of the plasma. The obtained field shape suggests that the induced electric field in the plasma when the electrodes are charged is

2013 JINST 8 P02005

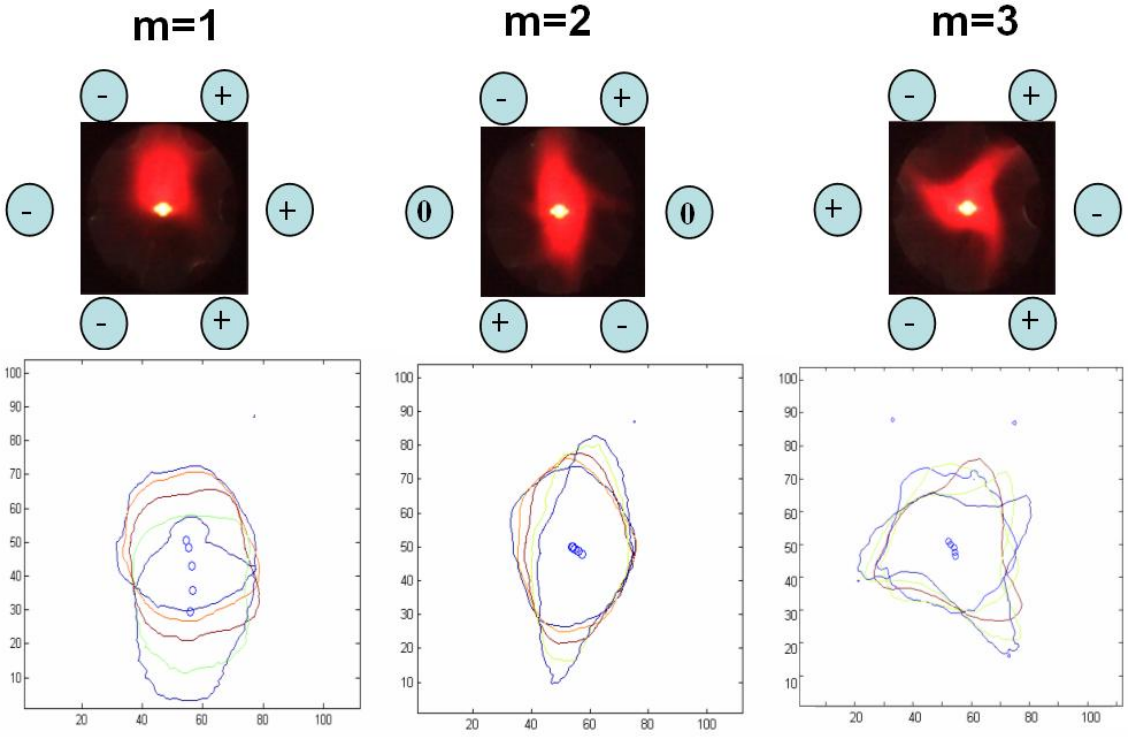

Figure 5. Top: the charging geometry of the electrodes (grey circles) and the resulting typical plasma shape. Bottom: equi-luminescence contours for 5 consecutive frames, demonstrating the plasma evolution in each case.

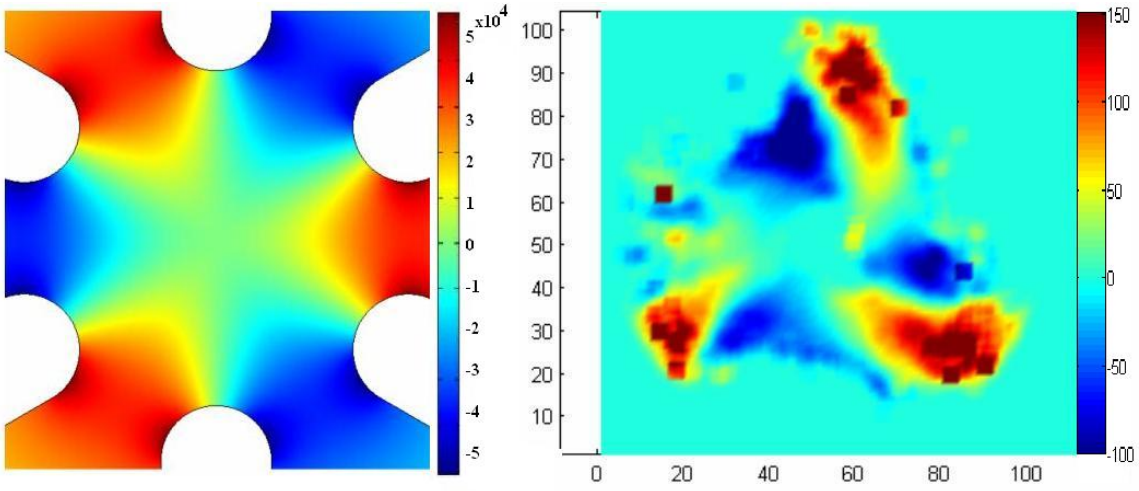

Figure 6. Left: calculated radial electric field of the electrodes in vacuum. Right: the measured electric field in the plasma. Note the difference of the color bars.

also affected by internal charge accumulation due to centrifugal drift, and plasma rotation due to radial electric field. These non-linear phenomena make the modeling of feedback with electrostatic fields very complicated.

2013 JINST 8 P02005

References

[1] A.I. Morozov and L.S. Solov'ev, *Cybernetic Stabilization of Plasma Instabilities*, *Sov. Phys. Tech. Phys.* **9** (1965) 1566.

[2] V.A. Chuyanov and E.G. Murphy, *Feedback Experiments on a High-Energy Plasma in the Phoenix Mirror Machine*, *Nuc. Fus.* **12** (1972) 177.

[3] V.A. Zhil'tsov, P.M. Kosarev, V.K. Likhtenshtein, D.A. Panov, V.Y. Chuyanov and A.G. Shcherbakov, *Limitations on the plasma density in the Ogra-3 device*, *Sov. J. Plasma Phys.* (Engl. transl.) **3** (1975) 20.

[4] A.D. Beklemishev, P.A. Bagrayansky, M.S. Chaschin and E.I. Soldatkina, *Vortex confinement of plasmas in symmetric mirror traps*, *Fus. Sci. Tech.* **57** (2010) 351.

[5] E.I. Soldatkina, P.A. Bagryansky and A.L. Solomakhin, *Influence of the Radial Profile of the Electric Potential on the Confinement of a High β Two-Component Plasma in a Gas-Dynamic Trap*, *Plasma Phys. R.* **34** (2008) 259.

[6] S.J. Zweben et al., *High-speed imaging of edge turbulence in NSTX*, *Nucl. Fus.* **44** (2004) 134.

[7] J.H. Yu and M.A. Zeeland, *Spectrally filtered fast imaging of internal magnetohydrodynamic activity in the DIII-D tokamaka*, *Rev. Sci. Inst.* **79** (2008) 10F516.

[8] S. Oldenbürger, F. Brochard and G. Bonhomme, *Investigation of mode coupling in a magnetized plasma column using fast imaging*, *Phys. Plasmas* **18** (2011) 032307.

[9] I.U. Uzun-Kaymak et al., *Cross-field plasma injection into mirror geometry*, *Plasma Phys. Control. Fus.* **51** (2009) 095007.

[10] NIST Atomic Spectra Database, http://www.nist.gov/pml/data/asd.cfm.

[11] R.J. Goldston and P.H. Rutherford, *Introduction to Plasma Physics*, Institute of Physics Publishing, Bristol (1995).

[12] M.Z. Caponi, B.I. Cohen and R.P. Freis, *Stabilization of the Flute Modes by Finit-Larmor-Radius and Surface Effects*, *Phys. Fluids* **30** (1987) 1410.

[13] M.N. Rosenbluth and C.L. Longmire, *Stability of plasmas confined by magnetic fields*, *Ann. Phys.* **1** (1957) 120.

[14] C. Janicki, R. Décoste, and C. Simm, *High-Resolution Soft-X-Ray Tomography of Sawtooth Oscillations on the Tokamak de Varennes*, *Phys. Rev. Lett.* **62** (1989) 3038.

2013 JINST 8 P02005